

Extraction of auroral oval boundaries from UVI images: A new FLICM clustering-based method and its evaluation

WANG Qian¹, MENG QingHu¹, HU ZeJun^{2*}, XING ZanYang^{2,3}, LIANG JiMin^{1*}
& HU HongQiao²

¹School of Life Sciences and Technology, Xidian University, Xi'an 710071, China;

²SOA Key Laboratory for Polar Science, Polar Research Institute of China, Shanghai 200136, China;

³School of Science, Xidian University, Xi'an 710071, China

Received June 28, 2011; accepted August 16, 2011

Abstract Based on the fuzzy local information c -means (FLICM) clustering algorithm, a new method is developed for extracting the equatorward and poleward boundaries of the auroral oval from images acquired by the Ultraviolet Imager (UVI) aboard the POLAR satellite. First, the method iteratively segments the UVI image with the FLICM clustering algorithm, according to an integrity criterion for the segmented auroral oval. Then, possible gaps in the extracted auroral oval are filled, based on prior knowledge of its shape. To evaluate the method objectively, the extracted boundaries are compared with the precipitating electron boundaries determined from DMSP satellite precipitation particle data. The evaluation results demonstrate that the proposed method generates more accurate auroral boundaries than traditional methods.

Keywords Auroral boundary, UVI, image segmentation, evaluation

Citation: Wang Q, Meng Q H, Hu Z J, et al. Extraction of auroral oval boundaries from UVI images: A new FLICM Clustering-based method and its evaluation. *Adv Polar Sci*, 2011, 22: 184–191, doi: 10.3724/SP.J.1085.2011.00184

0 Introduction

Aurorae are natural lights in the upper atmosphere that are produced by collisions between energetic particles precipitating from space with atoms or molecules in the upper atmosphere. Observations from remote imager instruments aboard satellites usually show the lights to have the shape of an annular ring centered on the Earth's magnetic poles, and they are called auroral ovals^[1–2]. Compared with local auroral observations from ground-based cameras, auroral images acquired by the Ultraviolet Imager (UVI) aboard the POLAR satellite can provide global auroral information, e.g., the overall configuration of the oval and spatial distribution of auroral

intensity along the oval. The equatorward and poleward boundaries of the auroral oval in UVI images, referred to as UVI boundaries, are closely related to the energy coupling between solar wind and the magnetosphere. The boundaries expand and contract in response to geomagnetic and solar wind activity^[3]. For auroral study, it is important to accurately extract the boundaries of the auroral oval.

To make full use of the large number of UVI images, automatic image segmentation methods for extracting auroral oval boundaries are of great appeal, because manually determining the auroral oval of so many images is tedious and impractical. Several methods have been

*Corresponding authors: (Hu Zejun, email: huzejun@pric.gov.cn; Liang Jimin, email: jimleung@mail.xidian.edu.cn)

presented in recent decades. These include threshold-based methods^[4–5], a histogram-based k -means algorithm^[6], an adaptive thresholding technique^[7], a pulse-coupled neutral network^[3] and shape-based methods^[8–9]. The methods of references[4–7] do not exploit auroral oval shape information and the spatial relationship of pixels. Therefore, they are unable to detect the complete auroral oval for some images, especially those with large auroral intensity variations. Cao et al.^[8–9] presented a shape-based method for extracting auroral ovals. They first segmented auroral images using the algorithm of Li et al.^[7], then selected some inner and outer boundary points from the resultant foreground, via radial-based processing. Finally, two ellipses fitted to the points using linear least-squares randomized Hough transform^[9] were used as the equatorward and poleward boundaries, respectively. Although this method produces complete boundaries of the auroral oval, it may introduce errors if the boundaries are not strictly elliptical, or if only parts of the auroral oval are imaged.

In this paper, a new approach for extracting the UVI boundaries is proposed, based on fuzzy local information c -means clustering (FLICM)^[10]. In this method, the UVI image is iteratively segmented according to an integrity measurement of the extracted auroral oval using FLICM, then auroral oval gaps are filled based on prior knowledge of its shape. The method is not only applicable to images with whole auroral ovals, but also to images with partial ovals.

To objectively evaluate the performance of various algorithms, we defined particle precipitation boundaries (called DMSF boundaries) derived from DMSF satellite observations^[11] as the real boundaries of the auroral oval. The comparative experimental results demonstrate that the method outperforms previous methods.

1 Auroral oval extraction based on fuzzy clustering

Auroral oval boundaries are usually blurry because of strong background noise. Fuzzy clustering techniques are a good choice for UVI image segmentation. These techniques have been studied extensively and applied successfully in many fields^[12–15]. In this paper, fuzzy local information c -means clustering (FLICM)^[10] is used to segment the auroral oval in a UVI image. FLICM uses a

fuzzy local (both spatial and gray level) similarity measure to overcome the disadvantages of traditional fuzzy c -means algorithms.

To extract a complete and accurate auroral oval from a UVI image, our method contains three main steps: image preprocessing; auroral oval segmentation using FLICM; and gap filling, based on prior knowledge of the auroral oval shape.

1.1 UVI image preprocessing

Effective preprocessing of the original UVI images greatly aids the accurate extraction of auroral ovals, especially for images with strong noise. The characteristics of UVI images include blurry and elliptical outer boundaries^[9], blurry inner boundaries with complex shapes, and the spatial distributions of the auroral oval centered on the Earth's magnetic poles, within a certain range (57.5° to 67° ^[16]) of magnetic latitude. We considered these characteristics in the UVI image preprocessing, as follows.

(1) Background removal. Pixels corresponding to magnetic latitudes less than 50° were removed.

(2) Negative pixel clearance. Pixels with negative gray values, possibly caused by noise, were set to zero.

(3) Small bright spot smoothing. A bright spot is defined as a connected region in which the pixel gray values are greater than a given threshold. The threshold T_g is defined as

$$T_g = \mu_A + 3\sigma_A \quad (1)$$

where μ_A and σ_A are the mean gray value and standard deviation of all pixels in the image, respectively. If the bright spot area is less than a predetermined threshold (20 pixels), the pixels inside the spot are set to the average value of pixels outside the spot and contained in the smallest rectangle covering the bright spot. Otherwise, the bright spot is not processed, to avoid destroying auroral substorm regions by mistake.

(4) Image smoothing. The pixels in each 3×3 neighborhood are partitioned into two classes, according to their gray values. The class with fewer pixels is considered the outlier, and its values are replaced by the average intensity of the other class.

Figure 1 demonstrates an example of the preprocessing steps. Figure 1(f) shows the effective image region. Only the data inside the effective region of the original image are meaningful.

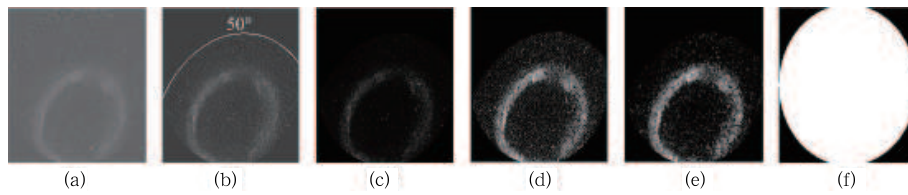


Figure 1 Preprocessing example. (a) Original UVI image. Images in (b) to (e) are preprocessed results of background removal, negative pixel clearance, small bright spot smoothing, and image smoothing, respectively. White region in last image (f) is the effective region of UVI image.

1.2 Auroral oval segmentation

After preprocessing, the UVI image is segmented into foregrounds (auroral regions) and backgrounds, using the FLICM method^[10]. The resultant auroral regions may be incomplete because of auroral intensity variation. To acquire a complete auroral oval from a UVI image, an integrity measurement T of the extracted foreground is defined as

$$T = \frac{\sum_{i=0}^m \theta(i)}{2\pi}, \quad 0 \leq \theta \leq 2\pi, m \geq 0 \quad (2)$$

where $\theta(i)$ represents the field angle of the i th connected foreground region, and $T \in [0, 1]$. If $T < \varepsilon$ (ε is a predetermined threshold), the background will be segmented again by FLICM. The resultant foregrounds are merged with former foreground regions, and the integrity T is recalculated. These procedures repeat until one of the following criteria is satisfied.

(1) $T=1$. This means the auroral oval has been completely extracted. We call this type of UVI image as class A.

(2) $\varepsilon \leq T < 1$ and the whole auroral oval is imaged (class B). The extracted auroral oval is incomplete and needs further postprocessing. Whether the entire auroral oval is imaged is assessed by the location of the fitted ellipse of the outer auroral oval boundary. If the fitted ellipse is completely inside the effective region of the UVI image, we conclude that the entire auroral oval is imaged.

(3) $\varepsilon \leq T < 1$ and only part of the auroral oval is

imaged (class C). The extracted auroral oval is incomplete, and will be postprocessed further.

(4) The number of segmentations by FLICM reaches the predetermined upper limit number β (class D).

Both class B and class C images are further postprocessed to generate complete auroral oval boundaries.

1.3 Auroral oval gap filling

For a class B image, the whole auroral oval is imaged, but not fully extracted, by iterative segmentation. An example is shown in Figure 2, where (a) is the original image and (b) is the segmented result. There is a gap on the segmented auroral oval that requires filling. Motivated by the annular ring characteristic of the auroral oval, Cao et al.^[9] used two ellipses fitted to the inner and outer boundaries to represent the equatorward and poleward boundaries, respectively. Here, we only fit the segmented outer boundary to an ellipse (the red ellipse in Figure 2(b)), and used it to fill the gap. The width of the gap is calculated as the linear interpolation of its starting and endpoint widths, which is defined as the average width of a small auroral oval section (10 degrees) adjacent to the gap. Figure 2(c) shows the filled gap, and Figure 2(d) shows the extracted auroral oval. After filling the gap, the inner and outer boundaries of the auroral oval were easily obtained.

The postprocessing of a class C image is similar to the procedures above, except that only the gaps of the auroral oval in the effective imaging region are filled. An example is shown in Figure 3.

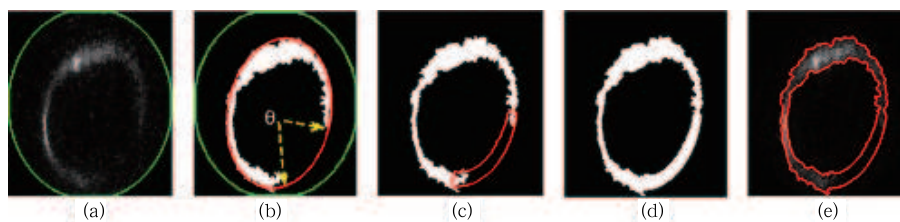


Figure 2 Example of gap filling of a B class image.

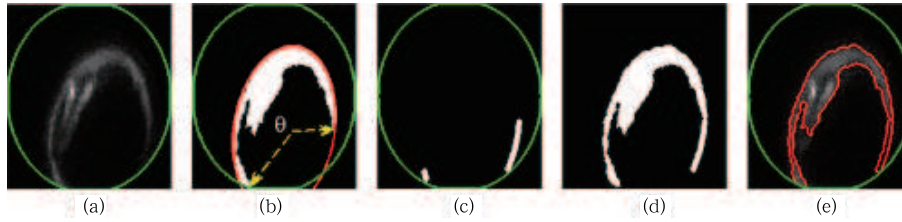


Figure 3 Example of gap filling of a C class image.

2 Evaluation

Subjective and objective evaluations of the performance of various methods for auroral oval segmentation were done. The five algorithms evaluated are AMET^[7], OTSU^[17], the classic FCM^[18], the method of Cao et al.^[9] (referred to as EF) and our method.

2.1 Subjective evaluation

Two type B images and two type C images were selected and segmented using the aforementioned five methods. For our method, the upper limit segmentation number was $\beta=4$ and the integrity threshold was $\varepsilon=0.65$. As shown in Figure 4, the auroral oval boundaries extracted by our method are more complete and accurate than those of the other methods. The AMET method considers pixel intensities within image zones. Its first step divides the UVI image into 24 sectors, based on magnetic

local time (MLT). Each sector spans 2 h, and has a 1 h overlap with the neighboring sectors. The thresholds calculated for each sector are smoothed, and then applied to the original image. This method tends to generate a “block effect”, because each subsector has a different threshold. The OTSU and classic FCM methods easily detect bright regions, but have difficulty in extracting aurorae with weak intensities. The EF method can delineate the closed inner and outer boundaries, but its precision needs improvement.

Figure 4 gives a preliminary impression of the performance of each method. To objectively evaluate the algorithms, we used the DMSP boundaries as the real auroral oval boundaries, as follows.

2.2 Objective evaluation

Cao et al.^[9] used manually-segmented auroral oval

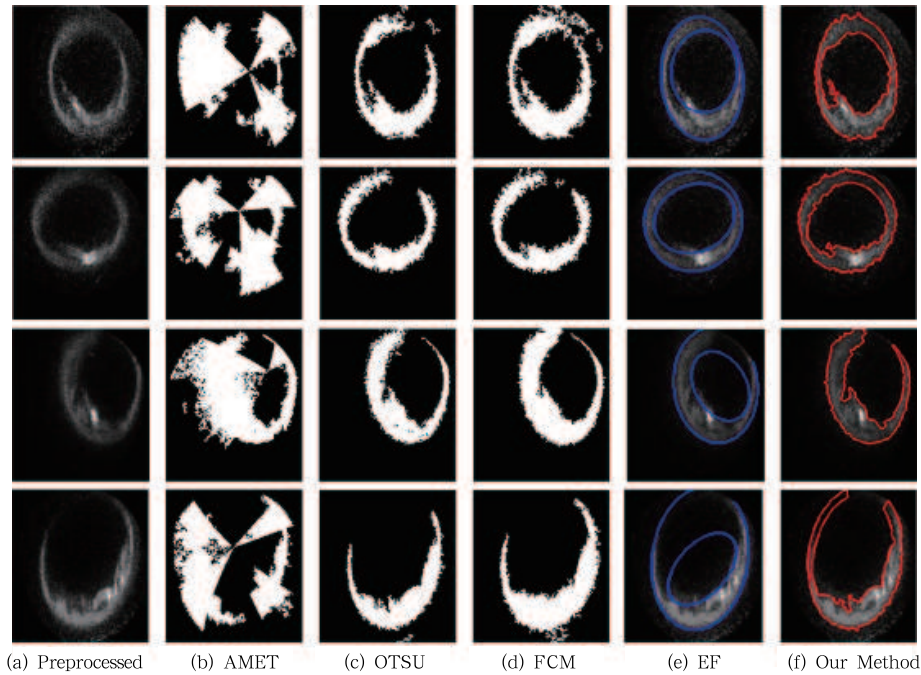


Figure 4 Auroral oval segmentation from the five methods. The first column (a) shows preprocessed UV images. Columns (b) to (f) are segmented images of AMET (b), OTSU (c), Classical FCM (d), EF (e) and our method (f), respectively. Blue and red curves in (e) and (f) indicate poleward and equatorward boundaries of the auroral oval.

boundaries as ground truth in an objective evaluation. However, manual determination of the auroral oval for a large number of images is tedious and impractical, and its results are subject to disagreement. Fortunately, precipitating electron boundaries can be distinguished by the DMSP satellite^[19–20], and some boundaries are closely related to UVI boundaries^[21–22]. To effectively evaluate methods of auroral boundary determination, we used the b1e and b6 boundaries defined by Newell et al.^[23–24] as the “real” equatorward and poleward boundaries, respectively. It should be noted that the UVI and DMSP satellites operate at different heights and measure different physical quantities. We call this bias as system bias. Therefore, auroral oval boundaries determined by these satellites are theoretically different, but the system bias doesn’t affect our evaluation.

2.2.1 Data

We used only nighttime UVI and DMSP data, since daytime auroral images were usually greatly affected by day-glow, which degrades the performance of existing methods in the extraction of aurora from UVI images^[9]. For nighttime, the b1e and b6 of Newell et al.^[23–24] were used to estimate the equatorward and poleward boundaries, respectively.

Two data sets were used in the evaluation. The first consists of global aurora images acquired by the Lyman-Birge-Hopfield long (LBHL) filter of UVI. These images have an accumulation time of 37 s over a sample interval of about 3 min. The second is from precipitating electrons detected by the SSJ/4 sensor on DMSP satellites. The detectors pointing toward the local zenith observe precipitating particles that cause auroral emissions on the trace of satellites. It is apparent that the UVI boundaries consist of two continuous curves (many pixels) in one image, while at the same time there may be just one sample dot in the DMSP data. In addition, the sample of an SSJ/4 sensor is not always simultaneous with the UVI image.

To match DMSP and UV boundaries effectively, we used the upper limits of time error and spatial deviations

between the two boundary types, denoted as M_t and M_d , respectively. The boundary matching procedures are as follows.

(1) The DMSP and UVI boundaries are converted to the same altitude-adjusted, corrected geomagnetic coordinates (AACGM), as described in Baker and Wing^[25].

(2) A selection is made of a point P at the DMSP boundary at time t . Its coordinate is $(Mlat, Mlt)$, where $Mlat$ and Mlt represent the magnetic latitude and magnetic local time, respectively.

(3) All UVI images captured during the period of $[t - M_t, t + M_t]$ are found.

(4) Images satisfying two of the following conditions are selected, to construct the basic matched image set.

a) The minimum Euclidean distances L_d , between P and every pixel in one image, must be less than M_d .

b) The pixel corresponding to L_d must be within the effective imaging region of the UVI images.

(5) $L_d(i)$ is Euclidean distance between P and the i th image in the basic matched image set. The UVI image with the minimum distance in $\{L_d(i)\}$ is assigned as the matched image of P .

The above steps are repeated until all DMSP boundaries are matched. Two matched databases are obtained, corresponding to the equatorward (Edata) and poleward (Pdata) auroral boundaries. These databases contain nighttime data during the polar night period from December, 1996 to January, 2000, about 11 months in total. Information on Edata and Pdata is shown in Table 1. Figure 5 shows distributions of equatorward and poleward boundaries with magnetic local time, magnetic longitude and magnetic latitude.

2.2.2 Evaluation experiments

Because the AMET^[7], OTSU^[17], and classical FCM^[18] methods cannot always generate complete auroral oval boundaries, we only compared our algorithm to the EF method^[9]. First, auroral boundaries were extracted using these two methods. The method precision is measured by the smallest distance error between the DMSP boundary point and the segmented UVI auroral

Table 1 Information on the evaluation database

Database	Edata	Pdata
Number of matches	961	922
Number of aurorae imaged completely (percentage)	266 (27.68 %)	270 (29.28 %)
Number of aurorae imaged incompletely(percentage)	695 (72.32 %)	652 (70.72 %)

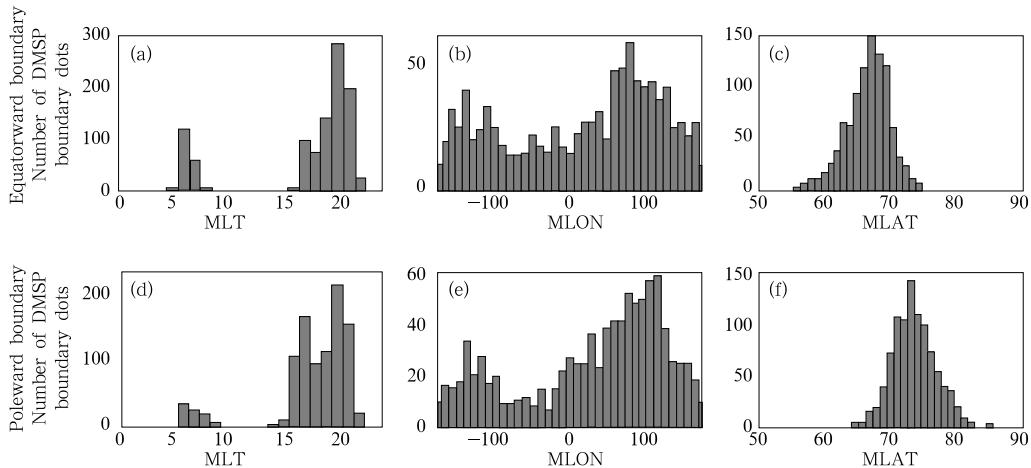


Figure 5 Distributions of equatorward and poleward boundaries with magnetic local time (MLT), magnetic longitude (MLON) and magnetic latitude (MLAT). Rows correspond to Edata and Pdata.

boundary points, which is defined as

$$D(Mlat, Mlt) = \sqrt{D_{-mlat}^2 + D_{-mlt}^2}, \quad (3)$$

$$D_{-mlat} = Mlat_{dmsp} - Mlat_{uv}, \quad (4)$$

$$D_{-mlt} = Mlt_{dmsp} - Mlt_{uv}, \quad (5)$$

where $(Mlat_{dmsp}, Mlt_{dmsp})$ are DMSP coordinates, and $(Mlat_{uv}, Mlt_{uv})$ are UVI boundary point coordinates, detected by EF or our method.

The statistical results of EF and our method, using the Edata and Pdata databases, are shown in Table 2,

where μ and σ indicate the mean and standard deviation of $D(Mlat, Mlt)$, respectively. From Table 2, we conclude that both equatorward and poleward boundaries from our method are more accurate than those from EF. The average equatorward and poleward boundary errors of the former method are less than 0.5.

Figure 6 depicts the error distribution of the equatorward and poleward boundaries determined by the two methods. The origin in the figures represents the “real” boundary determined by DMSP. This shows that the accuracy of the equatorward boundary from the EF method

Table 2 Statistical boundary detection errors of EF and our method

Method	Database	
	Edata	Pdata
EF method (μ, σ)	(0.7019, 0.6654)	(1.0646, 0.9275)
Our method (μ, σ)	(0.4542, 0.4244)	(0.4951, 0.4239)

is greater than that of the poleward boundary. The reason for this may be that most poleward boundaries do not have a strictly elliptical shape. Our method has similar accuracies for both equatorward and poleward boundary detection.

3 Conclusion

We present an approach to extract auroral oval boundaries from UVI images. The approach features an iterative segmentation of the auroral oval using the FLICM clustering algorithm, followed by gap filling based on prior information about the auroral oval shape. The

proposed method is applicable to UVI images with either complete or partial imaging of auroral ovals. The method can be easily extended to other kinds of global aurora images. In addition, an effective evaluation method is described, which assumes that DMSP boundaries represent the “real” auroral oval boundaries. The evaluation results show that our method is more accurate than previous methods in the extraction of the auroral oval.

The proposed method has been tested only on nighttime data. If strong dayglow is present, performance may deteriorate. To overcome this deficiency, blind signal separation techniques may be applied in the preprocessing stage, to remove interference from dayglow.

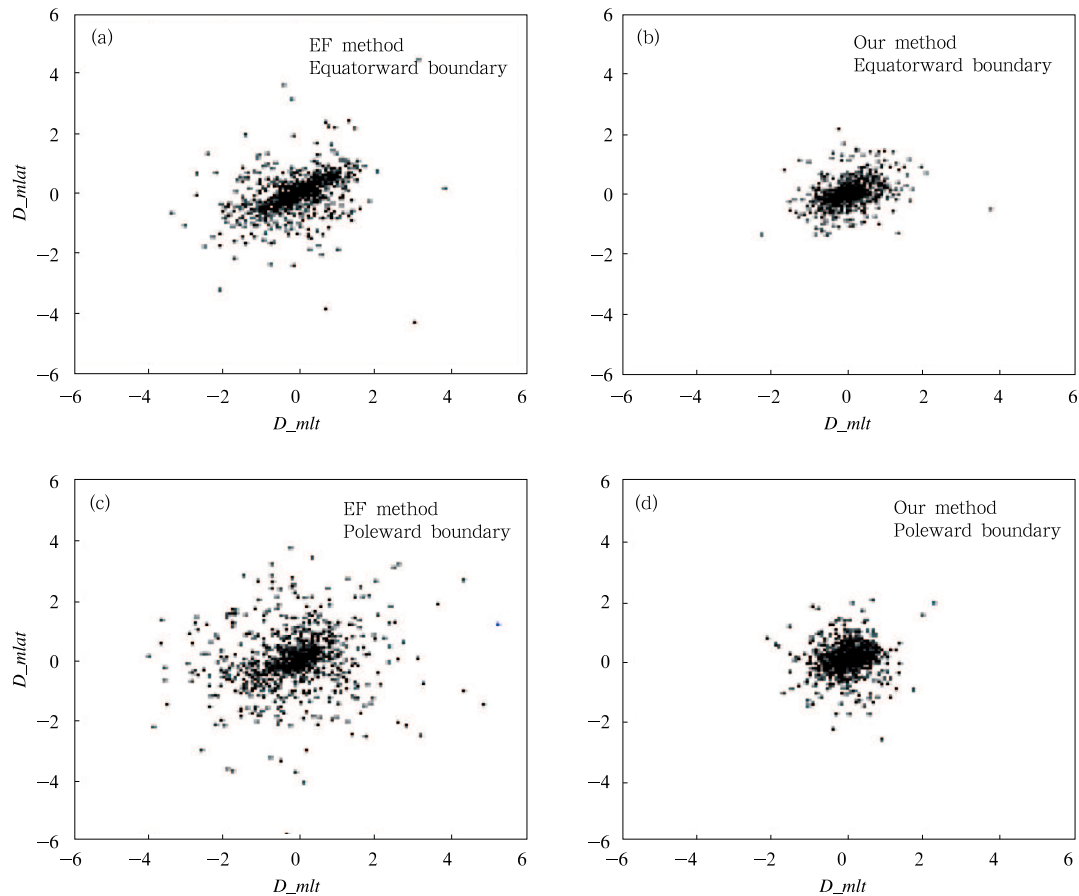


Figure 6 Distributions of equatorward and poleward boundary errors for EF-based method and our method in Edata (a, b) and Pdata (c, d).

Acknowledgments We are thankful to the Johns Hopkins University Applied Physics Laboratory and National Space Science and Technology Center (NSSTC) in Huntsville for the provision of DMSP and UVI data, respectively. This research was supported by the National Natural Science Foundation of China (Grant nos. 60872154, 41031064, 40904041, 40974103), the National High Technology Research and Development Program of China (Grant no. 2008AA121703) and the Ocean Public Welfare Scientific Research Project, State Oceanic Administration of China (Grant no. 201005017).

References

- 1 Akasofu S I. The latitudinal shift of the auroral belt. *Journal of Atmospheric and Terrestrial Physics*, 1964, 26(12): 1167–1174
- 2 Feldstein Y I. Some problems concerning the morphology of auroras and magnetic disturbances at high latitudes. *Geomagnetism Aeronomy*, 1963, 3: 183–192
- 3 Germany G A, Parks G K, Ranganath H, et al. Analysis of auroral morphology: substorm precursor and onset on January 10, 1997. *Geophysical Research Letters*, 1998, 25(15): 3042–3046
- 4 Frank L A, Craven J D. Imaging results from Dynamics Explorer 1. *Reviews of Geophysics*, 1988, 26(2): 249–283
- 5 Brittnacher M, Gillingim M, Parks G, et al. Polar cap area and boundary motion during substorms. *Journal of Geophysical Research*, 1999, 104(A6): 12251–12262
- 6 Hung C, Germany G. K-means and iterative selection algorithms in image segmentation. *IEEE Southeastcon 2003 (Session 1: Software Development)*
- 7 Li X, Ramachandran R, He M, et al. Comparing different thresholding algorithms for segmenting auroras. *Proceedings of the International Conference on Information Technology: Coding and Computing*, 2004, 6: 594–601
- 8 Cao C, Newman T S, Germany G. A shape-based technique for aurora oval segmentation from uvi images. *American Geophysical Union, Fall Meeting*, 2005
- 9 Cao C, Newman T S, Germany G. A new shape-based auroral oval segmentation driven by LLS-RHT. *Pattern Recognition*, 2009, 42: 607–618
- 10 Krinidis S, Chatzis V. A robust fuzzy local information c-means clustering algorithm. *IEEE Transaction on Image Processing*, 2010, 19(5): 1328–1337
- 11 Newell P T, Sotirelis T, Ruohoniemi J M, et al. OVATION: Oval Variation, Assessment, Tracking, Intensity, and Online

- Nowcasting. *Annales Geophysicae*, 2002, 20(7): 1039–1047
- 12 Yang M S. A survey of fuzzy clustering. *Mathematical and Computer Modelling*, 1993, 18(11): 1–16
 - 13 Delbo S, Gamba P, Roccatto D. A fuzzy shell clustering approach to recognize hyperbolic signatures in subsurface radar images. *IEEE Transactions on Geoscience and Remote Sensing*, 2000, 38(3): 1447–1451
 - 14 Dell’Acqua F, Gamba P. Detection of urban structures in SAR images by robust fuzzy clustering algorithms: the example of street tracking. *IEEE Transactions on Geoscience and Remote Sensing*, 2001, 39(10): 2287–2297
 - 15 Amini L, Soltanian-Zadeh H, Lucas C, et al. Automatic segmentation of thalamus from brain MRI integrating fuzzy clustering and dynamic contours. *IEEE Transactions on Biomedical Engineering*, 2004, 51(5): 800–811
 - 16 Galand M, Lummerzheim D, Stephan A W, et al. Electron and proton aurora observed spectroscopically in the far ultraviolet. *Journal of Geophysical Research*, 2002, 107(A7), doi: 10.1029/2001JA000235
 - 17 Otsu N. A threshold selection method from gray-Level histograms. *IEEE Transactions on Systems, Man, and Cybernetics*, 1979, 9(1): 62–66
 - 18 Bezdek J. *Pattern recognition with fuzzy objective function algorithms*. New York: Plenum Press, 1981
 - 19 Gussenhoven M S, Hardy D A, Burke W J. DMSP/F2 electron observations of equatorward auroral boundaries and their relationship to magnetospheric electric fields. *Journal of Geophysical Research*, 1981, 86(A2): 768–778
 - 20 Hardy D A, Burke W J, Gussenhoven M S, et al. DMSP/F2 electron observations of equatorward auroral boundaries and their relationship to the solar wind velocity and the north-south component of the interplanetary magnetic field. *Journal of Geophysical Research*, 1981, 86(A12): 9961–9974
 - 21 Carbary J F, Sotirelis T, Newell P T, et al. Auroral boundary correlations between UVI and DMSP. *Journal of Geophysical Research*, 2003, 108(A1), doi: 10.1029/2002JA009378
 - 22 Baker J B, Clauer C R, Ridley A J, et al. The nightside poleward boundary of the auroral oval as seen by DMSP and the Ultraviolet Imager. *Journal of Geophysical Research*, 2000, 105(A9): 21267–21280
 - 23 Newell P T, Feldstein Y I, Galperin Y I, et al. The morphology of nightside precipitation. *Journal of Geophysical Research*, 1996, 101(A5): 10737–10748
 - 24 Newell P T, Feldstein Y I, Galperin Y I, et al. Correction to “Morphology of nightside precipitation”. *Journal of Geophysical Research*, 1996, 101(A8): 17419–17421
 - 25 Baker K B, Wing S. A new magnetic coordinate system for conjugate studies at high latitudes. *Journal of Geophysical Research*, 1989, 94(A7): 9139–9143